Published in IET Microwaves, Antennas & Propagation
Received on 5th June 2011
Revised on 29th October 2011
doi: 10.1049/iet-map.2011.0264

ISSN 1751-8725

Modified wavefront decomposition method for fast and accurate ray-tracing simulation

V. Mohtashami A.A. Shishegar

Department of Electrical Engineering, Sharif University of Technology, Tehran, Iran
E-mail: shishegar@sharif.edu; mohtashami@ee.sharif.edu

Abstract: This study presents the modified wavefront decomposition method as a new ray-tracing acceleration technique for indoor propagation modelling. In this method, the exact propagation paths of the rays that reach the receiver after multiple reflections and/or refractions are calculated. Thus, the electromagnetic field at the receiver is obtained with a high accuracy. When only reflections are considered, our method simplifies to the multiple image theory or shooting and bouncing ray/image approach already available in the literature. However, the modified wavefront decomposition method calculates the exact propagation paths toward the receiver even if the rays encounter multiple refractions or a sequence of reflections and refractions. This novel contribution is specially important in indoor applications where through-the-wall propagation is usually noticeable. The significance of the proposed method is that the accuracy in the received field is obtained by shooting a few rays to the space around the transmitter. Consequently, a considerable reduction of the simulation time is achieved. The simulations show that the proposed method outperforms the traditional wavefront decomposition method. Furthermore, concurrent application of the proposed method and the previously published acceleration techniques is shown possible, which results in simulation time reduction of more than 11 times for a typical simulated indoor environment.

1 Introduction

Accurate multipath propagation modelling in complex indoor environments is a crucial prerequisite of designing reliable wireless personal and local area networks. Site-specific methods based on ray tracing have been proven to be versatile means for characterisation of wave propagation in indoor wireless channels [1–5]. However, despite being accurate and providing deep physical insight to the propagation mechanisms, ray tracing still suffers from long simulation time. Therefore a lot of research activities have been conducted over the past two decades in order to develop a fast and accurate ray-tracing method [6, 7].

There are basically two different types of ray tracing: image method [1, 4, 5] and shooting and bouncing ray (SBR) method [2]. The most important privilege of the image method is its high accuracy because it finds the exact propagation paths from the transmitter to the receiver. However, the computational burden of the image method grows exponentially with the number of the walls of the environment [1]. Thus, its application is limited to simple environments. The SBR method, on the other hand, is computationally efficient for complex environments and can well model the refraction phenomenon. These advantages make the SBR method the preferred technique for the study of indoor propagation where through-the-wall propagation is important. However, this type of ray tracing is less accurate than the image method because of the finite number of launched rays. The combination of the two ray-tracing methods has also been reported [3, 8, 9], which tries to take advantage of the accuracy of the image method and the computational efficiency of the SBR method. However, they have not modelled refraction and therefore their indoor application is limited to one-room scenarios and corridors.

In order to increase the accuracy of the SBR method, a lot of rays have to be launched from the transmitter. This, in turn, increases the simulation time. A group of acceleration techniques try to reduce the simulation time by incorporating bounding volumes or by rectangular and triangular meshing of the environment. Such methods reduce the intersection test calculations and the simulation time as reported in [7, 10–13]. In other research activities the concept of spatial super-sampling is used to reduce the simulation time [9, 14]. Nevertheless, the reduction in the simulation time is also achievable through an intelligent reduction of the number of the emitted rays as described in the next paragraph.

In a previous research conducted by the authors [15, 16], it was found that in typical indoor environments a relatively large number of emitted rays do not reach the receiver and hence tracing them is useless. The wavefront decomposition method utilises this fact and reduces the simulation time in an iterative manner. In the first iteration, a few rays are emitted from the source and traced. Then the detected rays at the receiver are found. The source rays corresponding to the detected rays have transported the transmitter power to the receiver and hence are called power-transporting source rays. The wavefronts of the power-transporting source rays are then decomposed to similar smaller wavefronts, which represent higher resolution for the source. Tracing the newly generated source rays and then decomposing the wavefronts of the power-transporting ones are iteratively

repeated until a high enough resolution is met. Since the resolution of the source is only increased for power-transporting source rays, runtime saving is achieved.

The purpose of the current paper is to present a new acceleration technique for SBR tracing. By preparing a mathematical framework, a fundamental modification is applied on the wavefront decomposition method. The exact propagation paths from the transmitter to the receiver can be found in a single iteration and by launching just a few rays. The proposed formulation allows considering multiple reflections and/or refractions and finds the propagation paths with the same high accuracy as the image method provides for multiple reflected rays. In other words, excellent accuracy is efficiently achieved for all multipath rays that arrive at the receiver. The modified wavefront decomposition method can also be concurrently used with the previously published acceleration techniques such as binary space partitioning (BSP) [11] and triangular grid ray tracing (TGRT) method [13] to yield further speedup.

The rest of the paper is organised as follows. In Section 2, the fundamental idea of the modified wavefront decomposition method is presented. It is shown that the representation of electromagnetic energy tubes by three rays can be used to store any arbitrary ray direction. Section 2 also develops the concept of expansion coefficients which will be used by Sections 3 and 4 to find the exact propagation paths of the energy tubes toward the receiver. Next, the modified wavefront decomposition method is presented in Section 5. It actually describes the efficient implementation of the derived formulas in ray tracing. The benefits of the method are also highlighted. Numerical results and simulation time reductions are reported in Section 6. A summary and important conclusions are given in Section 7.

2 Fundamental idea

In the traditional SBR tracing method, each emitted source ray represents an electromagnetic energy tube with spherical wavefront and circular cross section [2]. The energy tube is described by its axis in the direction of the emitted ray. As the ray propagates, its wavefront enlarges and if it illuminates the receiver location, its contribution to the total electromagnetic field at the receiver is considered. However, in most cases the receiver location does not lie on the axis of the wavefront as shown in Fig. 1*a*. At each intersection with the walls of the environment it is assumed that the interaction of the whole wavefront with the wall is described by the reflection or transmission coefficient calculated for its axis (ray). This causes some error since the correct path to the receiver encounters different incident

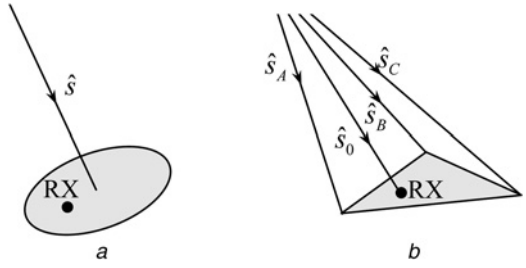

Fig. 1 *Energy tube representations*

a Representation by the axis (single ray)
b Representation by three rays

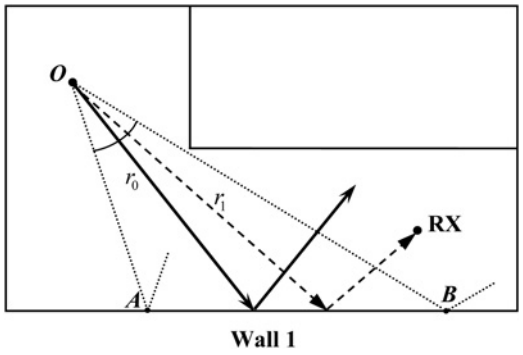

Fig. 2 *2D scenario in which the ray r_0 represents the energy tube $\widehat{AOB}$ and illuminates the receiver location after a single bounce at wall 1*

Exact path towards the receiver within $\widehat{AOB}$ is in the direction of r_1. 2D case is shown only for the sake of simplicity

angles compared to the axis (see Fig. 2). The reflection and refraction coefficients are therefore different for the correct path and the axis of the wavefront. Most objects in indoor environments are modelled as lossy dielectric media. Thus, the reflection and refraction coefficients have generally complex values. As a result, the received field which assumes the contribution of the electromagnetic field of the axis of the wavefront, contains both amplitude and phase errors. While both errors degrade the accuracy of the results, the impact of the phase error is much more severe since it causes inaccurate coherent summation of the electromagnetic fields of all received multipath components. The error increases when the receiver point is located farther from the axis.

If, however, an arbitrary vector inside an energy tube (which represents a potential ray direction) can be expressed using the information available for that energy tube, the correct path toward the receiver can be found through mathematical calculations. From linear algebra we know that any vector in the three-dimensional (3D) space can be completely described as a linear combination of three vectors that do not lie on the same plane. Thus, if we define each energy tube with three rays as shown in Fig. 1*b*, an arbitrary ray direction can be fully expressed as a linear combination of the directions of these three rays. This is mathematically expressed as

$$\hat{\mathbf{s}}_0 = \alpha_A \hat{\mathbf{s}}_A + \alpha_B \hat{\mathbf{s}}_B + \alpha_C \hat{\mathbf{s}}_C \tag{1}$$

where $\hat{\mathbf{s}}_A$, $\hat{\mathbf{s}}_B$ and $\hat{\mathbf{s}}_C$ are the directions of the three rays that define the energy tube, $\hat{\mathbf{s}}_0$ is the arbitrary vector inside the energy tube and α_A, α_B and α_C are the expansion coefficients. Without loss of generality, we consider $\hat{\mathbf{s}}_A$, $\hat{\mathbf{s}}_B$, $\hat{\mathbf{s}}_C$ and $\hat{\mathbf{s}}_0$ to be unit vectors. Under this assumption, the values of expansion coefficients are real and range between 0 and 1. Hereafter, we refer to $\{\hat{\mathbf{s}}_A, \hat{\mathbf{s}}_B, \hat{\mathbf{s}}_C\}$ as the characteristic vectors of the energy tube since any vector inside the energy tube is fully characterised by these three vectors. Note that the characteristic vectors form a solid angle. Thus, they are a basis for $\mathbb{R}^3$ space and linearly independent.

An energy tube may reach the receiver after several reflections and/or refractions. Thus, $\hat{\mathbf{s}}_A$, $\hat{\mathbf{s}}_B$ and $\hat{\mathbf{s}}_C$ change after each bounce at the walls of the environment. Let $\{\hat{\mathbf{s}}_A^{(k)}, \hat{\mathbf{s}}_B^{(k)}, \hat{\mathbf{s}}_C^{(k)}\}$ denote the characteristic vectors of an

doi: 10.1049/iet-map.2011.0264

arbitrary energy tube ($0 \le k \le M$). Each value of k represents the energy tube between two consecutive bounces, with $k = 0$ representing the energy tube at the transmitter location and $k = M$ representing the energy tube at the receiver location. An arbitrary vector inside this energy tube, denoted by $\hat{\mathbf{s}}_0^{(k)}$, can be expanded in terms of the characteristic vectors as

$$\hat{\mathbf{s}}_0^{(k)} = \alpha_A^{(k)}\hat{\mathbf{s}}_A^{(k)} + \alpha_B^{(k)}\hat{\mathbf{s}}_B^{(k)} + \alpha_C^{(k)}\hat{\mathbf{s}}_C^{(k)} \tag{2}$$

In other words, a set of $\{\alpha_A^{(k)}, \alpha_B^{(k)}, \alpha_C^{(k)}\}$ describes an arbitrary vector inside the energy tube for each value of k. Now, suppose that we perform a low-resolution ray tracing with a few energy tubes. If $\hat{\mathbf{s}}_0^{(M)}$ is interpreted as the correct path inside the energy tube towards the receiver (see Fig. 1*b*), the objective will be finding $\{\alpha_A^{(0)}, \alpha_B^{(0)}, \alpha_C^{(0)}\}$ for that energy tube, that is, the expansion coefficients at the transmitter location. If $\{\alpha_A^{(0)}, \alpha_B^{(0)}, \alpha_C^{(0)}\}$ are found, the exact path towards the receiver can be simply established by tracing $\hat{s}_0^{(0)}$. Furthermore, since only a few rays have been traced, a large saving in the simulation time is achieved. The modified wavefront decomposition method utilises this representation and finds the exact propagation paths from the transmitter to the receiver as described in the next three sections.

3 Formulation

The geometrical optics modelling of the objects in indoor environments involves dealing with the reflected and refracted rays at intersections with planar dielectric media. The objective of this section is to find the values of $\{\alpha_A^{(k+1)}, \alpha_B^{(k+1)}, \alpha_C^{(k+1)}\}$ as functions of $\{\alpha_A^{(k)}, \alpha_B^{(k)}, \alpha_C^{(k)}\}$. The derived formulas are then used in Section 4 to find the expansion coefficients $\{\alpha_A^{(0)}, \alpha_B^{(0)}, \alpha_C^{(0)}\}$ and to establish the correct path towards the receiver.

3.1 Reflection of the energy tube impinging on a dielectric half-space

Let $\{\hat{\mathbf{s}}_A^{(k)}, \hat{\mathbf{s}}_B^{(k)}, \hat{\mathbf{s}}_C^{(k)}\}$ and $\{\hat{\mathbf{s}}_A^{(k+1)}, \hat{\mathbf{s}}_B^{(k+1)}, \hat{\mathbf{s}}_C^{(k+1)}\}$ respectively denote the characteristic vectors of the incident and reflected energy tubes at $(k+1)$ th intersection ($k \ge 0$). Suppose that an arbitrary vector inside the incident energy tube, denoted by $\hat{\mathbf{s}}_0^{(k)}$, has been expanded in terms of the three incident characteristic vectors using (2). Also, let $\hat{\mathbf{s}}_0^{(k+1)}$ denote the reflected counterpart of $\hat{\mathbf{s}}_0^{(k)}$ and be expanded in terms of the characteristic vectors of the reflected energy tube as

$$\hat{\mathbf{s}}_0^{(k+1)} = \alpha_A^{(k+1)}\hat{\mathbf{s}}_A^{(k+1)} + \alpha_B^{(k+1)}\hat{\mathbf{s}}_B^{(k+1)} + \alpha_C^{(k+1)}\hat{\mathbf{s}}_C^{(k+1)} \tag{3}$$

This situation is depicted in Fig. 3*a*. Let the unit outward normal vector of the intersected wall be denoted by $\hat{\boldsymbol{n}}^{(k)}$. According to the Snell's law, the reflected rays can be calculated [17]. For instance

$$\hat{\mathbf{s}}_A^{(k+1)} = \hat{\mathbf{s}}_A^{(k)} - 2(\hat{\boldsymbol{n}}^{(k)} \cdot \hat{\mathbf{s}}_A^{(k)})\hat{\boldsymbol{n}}^{(k)} \tag{4}$$

Other reflected rays ($\hat{\mathbf{s}}_B^{(k+1)}$, $\hat{\mathbf{s}}_C^{(k+1)}$ and $\hat{\mathbf{s}}_0^{(k+1)}$) are calculated similarly. Substituting the reflected rays according to (4) in (3) and then using (2) in the resulting equation, we obtain

$$2(\hat{\boldsymbol{n}}^{(k)} \cdot \boldsymbol{l})\hat{\boldsymbol{n}}^{(k)} - \boldsymbol{l} = 0 \tag{5}$$

where

$$\boldsymbol{l} = (\alpha_A^{(k+1)} - \alpha_A^{(k)})\hat{\mathbf{s}}_A^{(k)} + (\alpha_B^{(k+1)} - \alpha_B^{(k)})\hat{\mathbf{s}}_B^{(k)} + (\alpha_C^{(k+1)} - \alpha_C^{(k)})\hat{\mathbf{s}}_C^{(k)}$$

By decomposing $\boldsymbol{l}$ and $\hat{\boldsymbol{n}}^{(k)}$ to their corresponding x-, y- and z-components ($\boldsymbol{l} = l_x\hat{\mathbf{x}} + l_y\hat{\mathbf{y}} + l_z\hat{\mathbf{z}}$ and $\hat{\boldsymbol{n}}^{(k)} = n_x\hat{\mathbf{x}} + n_y\hat{\mathbf{y}} + n_z\hat{\mathbf{z}}$), we can rewrite (5) as

$$\begin{bmatrix} 2n_x^2 - 1 & 2n_xn_y & 2n_xn_z \\ 2n_yn_x & 2n_y^2 - 1 & 2n_yn_z \\ 2n_zn_x & 2n_zn_y & 2n_z^2 - 1 \end{bmatrix} \begin{bmatrix} l_x \\ l_y \\ l_z \end{bmatrix} = \begin{bmatrix} 0 \\ 0 \\ 0 \end{bmatrix} \tag{6}$$

The determinant of the coefficient matrix of the equation system described by (6) equals $2(n_x^2 + n_y^2 + n_z^2) - 1$. Since $\hat{\boldsymbol{n}}^{(k)}$ is a unit vector, the determinant equals unity. Therefore, $\boldsymbol{l} = 0$ and since $\hat{\mathbf{s}}_A^{(k)}$, $\hat{\mathbf{s}}_B^{(k)}$ and $\hat{\mathbf{s}}_C^{(k)}$ are linearly independent, we must have $\alpha_A^{(k+1)} = \alpha_A^{(k)}$, $\alpha_B^{(k+1)} = \alpha_B^{(k)}$ and $\alpha_C^{(k+1)} = \alpha_C^{(k)}$. This means that the expression of $\hat{\mathbf{s}}_0^{(k+1)}$ in terms of $\{\hat{\mathbf{s}}_A^{(k+1)}, \hat{\mathbf{s}}_B^{(k+1)}, \hat{\mathbf{s}}_C^{(k+1)}\}$ is the same as the expression of $\hat{\mathbf{s}}_0^{(k)}$ in terms of $\{\hat{\mathbf{s}}_A^{(k)}, \hat{\mathbf{s}}_B^{(k)}, \hat{\mathbf{s}}_C^{(k)}\}$. In other words, the direction of a vector inside an energy tube relative to the directions of the characteristic vectors of that energy tube is not affected by specular reflection.

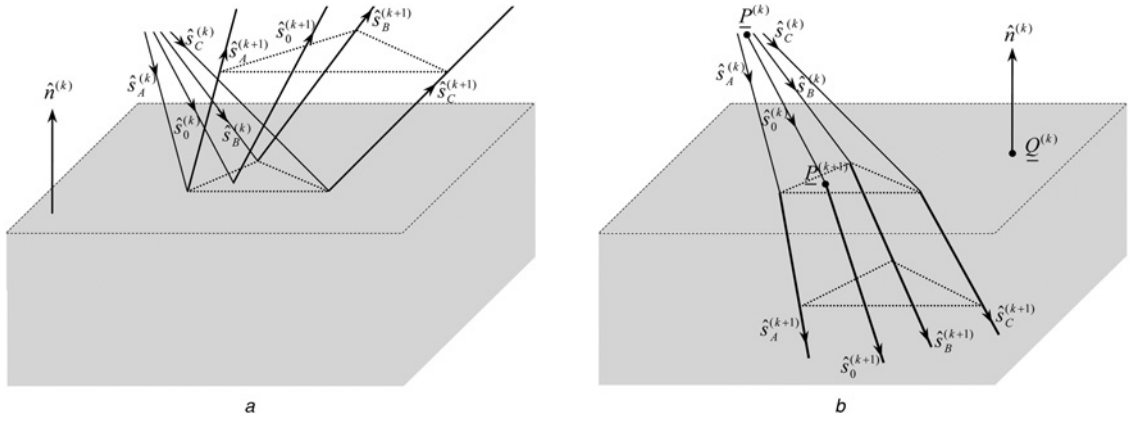

Fig. 3 *Interaction of an energy tube with a planar dielectric medium*
a Reflection
b Refraction

3.2 Refraction of the energy tube impinging on a dielectric half-space

Consider Fig. 3*b* that shows the refraction of an energy tube at the $(k+1)$ th intersection $(k \geq 0)$. In this case, let $\{\hat{\boldsymbol{s}}_A^{(k)}, \hat{\boldsymbol{s}}_B^{(k)}, \hat{\boldsymbol{s}}_C^{(k)}\}$ and $\{\hat{\boldsymbol{s}}_A^{(k+1)}, \hat{\boldsymbol{s}}_B^{(k+1)}, \hat{\boldsymbol{s}}_C^{(k+1)}\}$ denote the characteristic vectors of the incident and refracted energy tubes, respectively. The direction of each refracted ray can be obtained according to the Snell's law [17]. For instance

$$\hat{\boldsymbol{s}}_A^{(k+1)} = -\hat{\boldsymbol{n}}^{(k)} \cos\theta_A^{(k+1)} + m^{(k)}(\hat{\boldsymbol{s}}_A^{(k)} - (\hat{\boldsymbol{n}}^{(k)} \cdot \hat{\boldsymbol{s}}_A^{(k)})\hat{\boldsymbol{n}}^{(k)}) \quad (7)$$

where $m^{(k)}$ is the ratio of the refractive index of the kth medium to the $(k+1)$th medium and $\theta_A^{(k)}$ and $\theta_A^{(k+1)}$ are the incident and refraction angles, respectively. Other refracted rays are calculated similarly. We wish to find how the expansion coefficients of the refracted energy tube are related to their incident energy tube counterparts. To find this, we express $\hat{\boldsymbol{s}}_A^{(k+1)}$, $\hat{\boldsymbol{s}}_B^{(k+1)}$, $\hat{\boldsymbol{s}}_C^{(k+1)}$ and $\hat{\boldsymbol{s}}_0^{(k+1)}$ according to the Snell's law as in (7), insert them in (3), and then use (2) for expressing $\hat{\boldsymbol{s}}_0^{(k)}$. The result is a homogeneous equation in terms of a linear combination of $\{\hat{\boldsymbol{s}}_A^{(k)}, \hat{\boldsymbol{s}}_B^{(k)}, \hat{\boldsymbol{s}}_C^{(k)}\}$. Utilising the linear independence of $\{\hat{\boldsymbol{s}}_A^{(k)}, \hat{\boldsymbol{s}}_B^{(k)}, \hat{\boldsymbol{s}}_C^{(k)}\}$ we set their coefficients in the resulting equation to zero which yields

$$(\boldsymbol{U}^{(k)} + \boldsymbol{V}^{(k)})\boldsymbol{\alpha}^{(k+1)} = \boldsymbol{U}^{(k)}\boldsymbol{\alpha}^{(k)} + \boldsymbol{W}^{(k)} \quad (8)$$

where

$$\boldsymbol{\alpha}_{3\times1}^{(k)} = [\alpha_A^{(k)}\ \alpha_B^{(k)}\ \alpha_C^{(k)}]^t, \quad \boldsymbol{\alpha}_{3\times1}^{(k+1)} = [\alpha_A^{(k+1)}\ \alpha_B^{(k+1)}\ \alpha_C^{(k+1)}]^t$$

('t' denotes the transpose of matrix) and

$$\boldsymbol{U}_{3\times3}^{(k)} = m^{(k)}(\boldsymbol{I}_{3\times3} - [n_A^{(k)}\ n_B^{(k)}\ n_C^{(k)}]^t[\gamma_A^{(k)}\ \gamma_B^{(k)}\ \gamma_C^{(k)}]) \quad (9)$$

$$\boldsymbol{V}_{3\times3}^{(k)} = -[n_A^{(k)}\ n_B^{(k)}\ n_C^{(k)}]^t\,[\cos\theta_A^{(k+1)}\ \cos\theta_B^{(k+1)}\ \cos\theta_C^{(k+1)}] \quad (10)$$

$$\boldsymbol{W}_{3\times1}^{(k)} = -[n_A^{(k)}\ n_B^{(k)}\ n_C^{(k)}]^t(1 - (m^{(k)})^2\, g(\boldsymbol{\alpha}^{(k)}))^{1/2} \quad (11)$$

In (9)–(11)

$$\hat{\boldsymbol{n}}^{(k)} = n_A^{(k)}\hat{\boldsymbol{s}}_A^{(k)} + n_B^{(k)}\hat{\boldsymbol{s}}_B^{(k)} + n_C^{(k)}\hat{\boldsymbol{s}}_C^{(k)}, \quad \boldsymbol{I}_{3\times3}$$

is the 3×3 identity matrix

$$\gamma_A^{(k)} = \hat{\boldsymbol{n}}^{(k)} \cdot \hat{\boldsymbol{s}}_A^{(k)}, \quad \gamma_B^{(k)} = \hat{\boldsymbol{n}}^{(k)} \cdot \hat{\boldsymbol{s}}_B^{(k)}, \quad \gamma_C^{(k)} = \hat{\boldsymbol{n}}^{(k)} \cdot \hat{\boldsymbol{s}}_C^{(k)}$$

the refraction angles are denoted by

$$\theta_A^{(k+1)},\ \theta_B^{(k+1)},\ \theta_C^{(k+1)} \text{ and } g(\boldsymbol{\alpha}^{(k)}) = 1 - (\gamma_A^{(k)}\alpha_A^{(k)} + \gamma_B^{(k)}\alpha_B^{(k)} + \gamma_C^{(k)}\alpha_C^{(k)})^2$$

Given $\boldsymbol{\alpha}^{(k)}$, the value of $\boldsymbol{\alpha}^{(k+1)}$ can be calculated using (8). Note that (8) simplifies to $\boldsymbol{\alpha}^{(k+1)} = \boldsymbol{\alpha}^{(k)}$ for $m^{(k)} = 1$ as expected.

3.3 Reflection and transmission of the energy tube impinging on a dielectric slab

Many objects in the environment such as walls, ceiling and floor etc. are well modelled by dielectric slabs. In this case as depicted in Fig. 4*a*, the slab reflection and transmission coefficients are used instead of the Fresnel reflection and transmission coefficients. The effect of multiple reflections inside the slab is included in the slab reflection and transmission coefficients and multiple reflected and transmitted rays are replaced by a single reflected ray, and a single transmitted ray that leaves the other side of the slab [18] (see Fig. 4*a*). The characteristic vectors of the transmitted energy tube are parallel to their corresponding characteristic vectors of the incident energy tube. Hence, the values of the expansion coefficients remain unchanged after being transmitted to the other side of the slab. It should be noted that the slab case can be treated as multiple reflections and refractions between two half-space dielectric media and the formulations of the previous two subsections be used. However, by using the slab reflection and transmission coefficients, the formulations are greatly simplified.

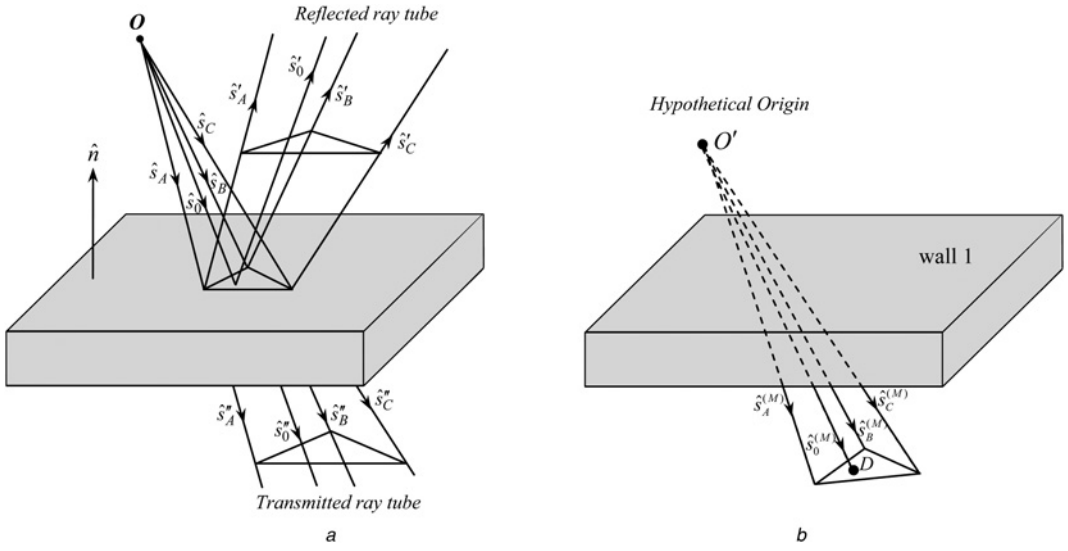

Fig. 4 *Slab case*

a Reflected and transmitted energy tubes
b Detection at the receiver

doi: 10.1049/iet-map.2011.0264

4 Path correction

The values of the expansion coefficients of the source ray which is supposed to pass through the exact location of the receiver, that is, $\{\alpha_A^{(0)}, \alpha_B^{(0)}, \alpha_C^{(0)}\}$, can be found using the formulas derived in Section 3 and considering the locations of the transmitter and the receiver. The intersection point of $\hat{\boldsymbol{s}}_0^{(k)}$ at the $(k+1)$th intersection, denoted by $\underline{P}^{(k+1)}$, $0 \leq k \leq M-1$, can be found as

$$\underline{P}^{(k+1)} = \underline{P}^{(k)} + \hat{\boldsymbol{s}}_0^{(k)} t^{(k)} \tag{12}$$

where $\underline{P}^{(k)}$ is the originating point of $\hat{\boldsymbol{s}}_0^{(k)}$ a (see Fig. 3*b*) which itself is the intersection point at the kth intersection, and $t^{(k)}$ is the distance between the $\underline{P}^{(k)}$ and $\underline{P}^{(k+1)}$. Note that $\underline{P}^{(0)}$ is the location of the transmitting antenna. According to the basic ray-tracing equations [10], we have

$$t^{(k)} = -\frac{\hat{\boldsymbol{n}}^{(k)} \cdot \underline{\boldsymbol{Q}}^{(k)} \underline{\boldsymbol{P}}^{(k)}}{\alpha_A^{(k)}\gamma_A^{(k)} + \alpha_B^{(k)}\gamma_B^{(k)} + \alpha_C^{(k)}\gamma_C^{(k)}} \tag{13}$$

where $\hat{\boldsymbol{n}}^{(k)}$ and $\underline{Q}^{(k)}$ are the normal vector and an arbitrary point of the $(k+1)$th intersected surface. Now, if the energy tube illuminates the receiver location, denoted by $\underline{R}$, after encountering M intersections, we have

$$\frac{\underline{\boldsymbol{P}}^{(M)}\underline{\boldsymbol{R}}}{\|\underline{\boldsymbol{P}}^{(M)}\underline{\boldsymbol{R}}\|} = \alpha_A^{(M)}\hat{\boldsymbol{s}}_A^{(M)} + \alpha_B^{(M)}\hat{\boldsymbol{s}}_B^{(M)} + \alpha_C^{(M)}\hat{\boldsymbol{s}}_C^{(M)} = \hat{\boldsymbol{s}}_0^{(M)} \tag{14}$$

where $\| \ \|$ denotes the Euclidean norm. In (14), the values of $\{\alpha_A^{(M)}, \alpha_B^{(M)}, \alpha_C^{(M)}\}$ and $\underline{P}^{(M)}$ are functions of $\{\alpha_A^{(0)}, \alpha_B^{(0)}, \alpha_C^{(0)}\}$ according to (8), (12), (13). Thus, (14) represents a 3×3 non-linear equation system in terms of $\{\alpha_A^{(0)}, \alpha_B^{(0)}, \alpha_C^{(0)}\}$. The solution can be very efficiently found using iterative Newton's method. Since we know that the values of $\{\alpha_A^{(0)}, \alpha_B^{(0)}, \alpha_C^{(0)}\}$ are between 0 and 1, a good choice for the initial value of $\boldsymbol{\alpha}^{(0)}$ is obtained by selecting $\alpha_A^{(0)} = \alpha_B^{(0)} = \alpha_C^{(0)}$. In our simulations, this choice resulted in very fast convergence of the Newton's method in two or three iterations.

There is a special case in which $\{\alpha_A^{(0)}, \alpha_B^{(0)}, \alpha_C^{(0)}\}$ can be found in a much simpler way as compared to the solution offered by Newton's method. It happens when the detected energy tube has encountered only dielectric slabs on its way towards the receiver. A situation in which the receiver falls within a transmitted energy tube is shown in Fig. 4*b*. In this figure, $\{\hat{\boldsymbol{s}}_A^{(M)}, \hat{\boldsymbol{s}}_B^{(M)}, \hat{\boldsymbol{s}}_C^{(M)}\}$ are the characteristic vectors of the transmitted energy tube for which the receiver, located at point D, falls within. According to the total unfolded path lengths travelled by $\{\hat{\boldsymbol{s}}_A^{(M)}, \hat{\boldsymbol{s}}_B^{(M)}, \hat{\boldsymbol{s}}_C^{(M)}\}$, the location of a hypothetical point, denoted by O', can be found from which these three vectors seem to have originated. Therefore O' can be thought as the hypothetical origin of the energy tube. The correct path direction towards the receiver is given by $\boldsymbol{O'D}$. Since both $\boldsymbol{O'}$ and $\boldsymbol{D}$ are known, the vector $\boldsymbol{O'D}$ is known as well. Let $\hat{\boldsymbol{s}}_0^{(M)}$ denote the unit vector in the direction of $\boldsymbol{O'D}$. We can use (2) to express $\hat{\boldsymbol{s}}_0^{(M)}$ in terms of $\{\hat{\boldsymbol{s}}_A^{(M)}, \hat{\boldsymbol{s}}_B^{(M)}, \hat{\boldsymbol{s}}_C^{(M)}\}$ to find $\{\alpha_A^{(M)}, \alpha_B^{(M)}, \alpha_C^{(M)}\}$. Since the energy tube has encountered only reflections and/or transmissions by slab, the values of the expansion coefficients do not change up to the receiver location and we have $\boldsymbol{\alpha}^{(0)} = \boldsymbol{\alpha}^{(M)}$. Hence, the path of the energy tube towards the receiver is corrected with a very simple mathematical calculation.

There exists a negligible approximation in the value of $\boldsymbol{\alpha}^{(M)}$ obtained above in the slab case. Owing to the effect of astigmatism [17] caused by refractions inside slabs, O' is not a point; rather it is a tiny triangle. However, since slab thicknesses are much less than the distances travelled by $\{\hat{\boldsymbol{s}}_A^{(M)}, \hat{\boldsymbol{s}}_B^{(M)}, \hat{\boldsymbol{s}}_C^{(M)}\}$, this triangle is always very small and selecting its centre of mass as O' yields accurate value for $\boldsymbol{\alpha}^{(M)}$.

5 Implementation of the algorithm

The purpose of this section is efficient implementation of the formulas derived in Sections 3 and 4 in ray tracing. The result

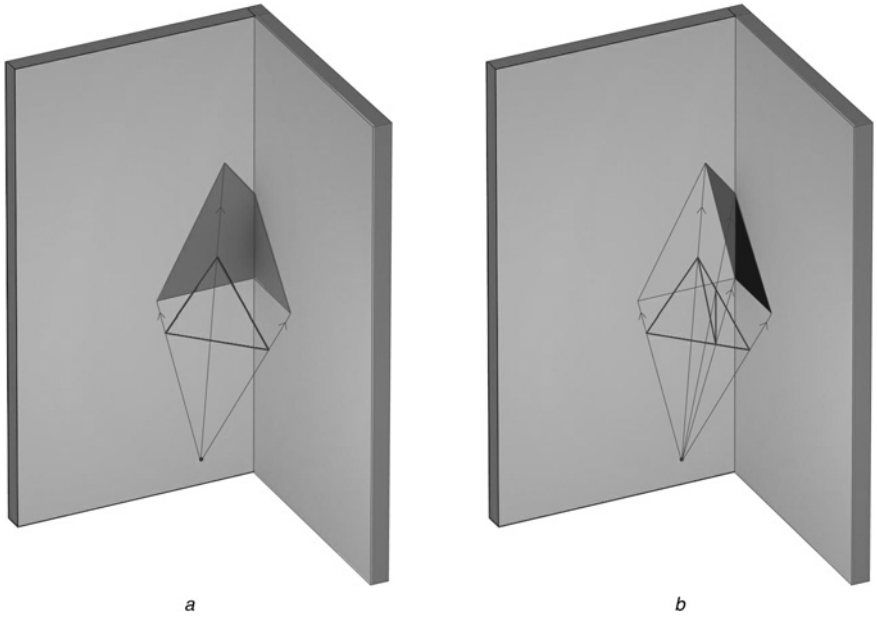

Fig. 5 *Example of wavefront decomposition scheme*

a Original wavefront illuminates two walls
b Decomposition to three smaller wavefronts each of which hits only one wall

will be an efficient and accurate ray tracing, which we call it the modified wavefront decomposition method.

An important condition that must always hold in the presented formulations is that all three characteristic vectors of an energy tube must hit the same wall at an intersection. As long as this condition holds, the correct path towards the receiver can be established. If this condition is violated, as illustrated in Fig. 5, the triangular wavefront can be simply decomposed into smaller triangular wavefronts such that each newly generated wavefront hits a single wall. In other words, the decomposition of wavefronts is performed during the ray-tracing procedure for a few energy tubes that illuminate more than one wall in a single intersection. Thus, the ray-tracing simulation can be started with a few energy tubes and the wavefronts be decomposed whenever necessary. By using this methodology, a lot of simulation time will be saved without compromising the accuracy. We refer to this methodology as the modified wavefront decomposition method. It finds the exact propagation paths in a single iteration and thus is more efficient than the traditional wavefront decomposition method [15, 16]. The flowchart of the method is depicted in Fig. 6.

The modified wavefront decomposition method has several interesting features:

1. Tracing each $\hat{s}_0^{(0)}$ has very low computational cost. This is because the sequence of walls intersected by the corresponding energy tube has been previously determined. Hence, no extra intersection test is required.
2. The modified wavefront decomposition method finds the exact propagation paths from the transmitter to the receiver for the line-of-sight (LOS) energy tube as well as the energy tubes that undergo a sequence of reflections and/or refractions. If only reflections are considered, our proposed method simplifies to published theories known as multiple image theory [8], SBR/image approach [3] or adaptive ray tube tracing [9]. While these published methods can find the exact propagation paths for multiple reflected rays, none of them deals with the refraction of rays. Hence, they are mostly used in outdoor applications or indoor scenarios involving a single room or corridors. The modified wavefront decomposition is more general in the sense that it also includes multiple refractions and hence accurately models the propagation through the walls. Therefore it can be used in general indoor environments in addition to the aforementioned indoor and and outdoor applications.
3. The modified wavefront decomposition method can also find the exact propagation path of a diffracted ray towards the receiver. When an energy tube hits a wedge and diffraction occurs, the wedge acts as a secondary source and emits diffracted energy tubes. Each diffracted energy tube can then be normally traced in the environment. If a diffracted energy tube illuminates the receiver (directly or after several bounces), the expansion coefficients at the wedge location can be found by solving (14) and the exact propagation path towards the receiver can be established.
4. The modified wavefront decomposition method can be used simultaneously with the bounding-volume-based acceleration techniques such as BSP [11] and with TGRT method [13]. The reason is that these methods reduce the computational cost of tracing each ray (per-ray speedup), whereas our presented method judiciously reduces the number of launched rays (ensemble speedup). Therefore, there will be no conflict if they are used concurrently and the total speedup will be the product of ensemble speedup and per-ray speedup. Hence, more reduction of simulation time is feasible.
5. The formulation of the modified wavefront decomposition method suppresses the necessity of uniformly generating the rays around the transmitter. In the traditional ray tracing, uniform generation of the source rays in the 3D space is required in order to unbiasedly include all possible routes from the transmitter to the receiver [2, 3]. However, in the modified wavefront decomposition method, we can simply tessellate the walls of the environment into very big triangles and send out the rays from the transmitter only in the directions pointing to the vertices of these triangles. The few resulting energy tubes will have large wavefronts, but we are sure that by decomposing the wavefronts whenever necessary, no possible propagation path is missed. This source modelling scheme automatically generates more energy tubes in directions where the geometry of the environment is more complex; that is, the spatial

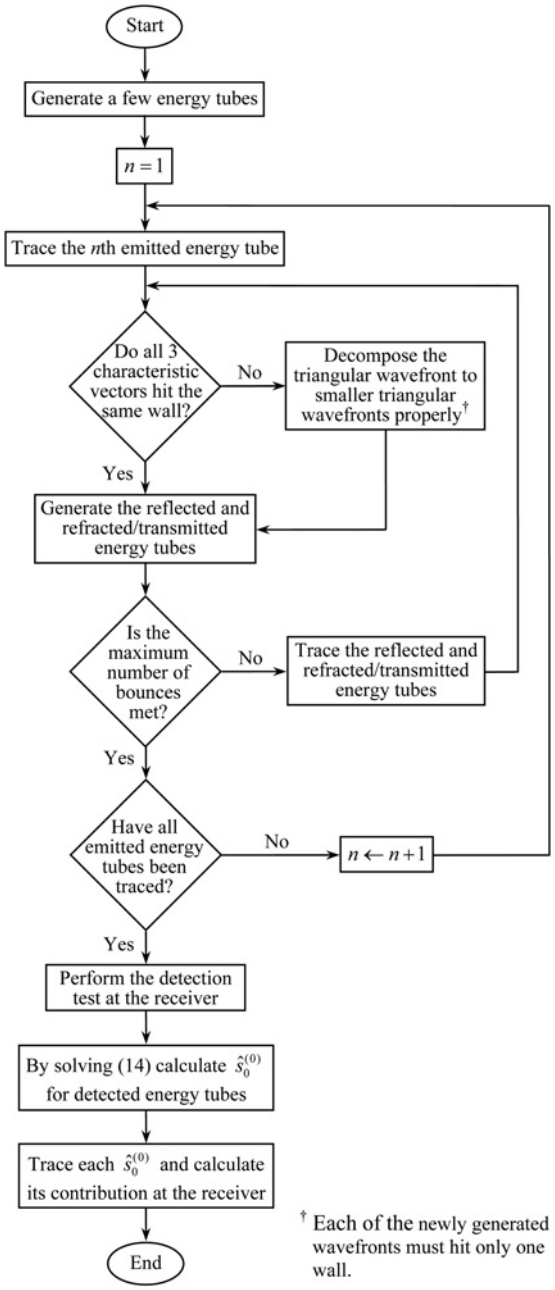

Fig. 6 *Flowchart of the modified wavefront decomposition method*

doi: 10.1049/iet-map.2011.0264

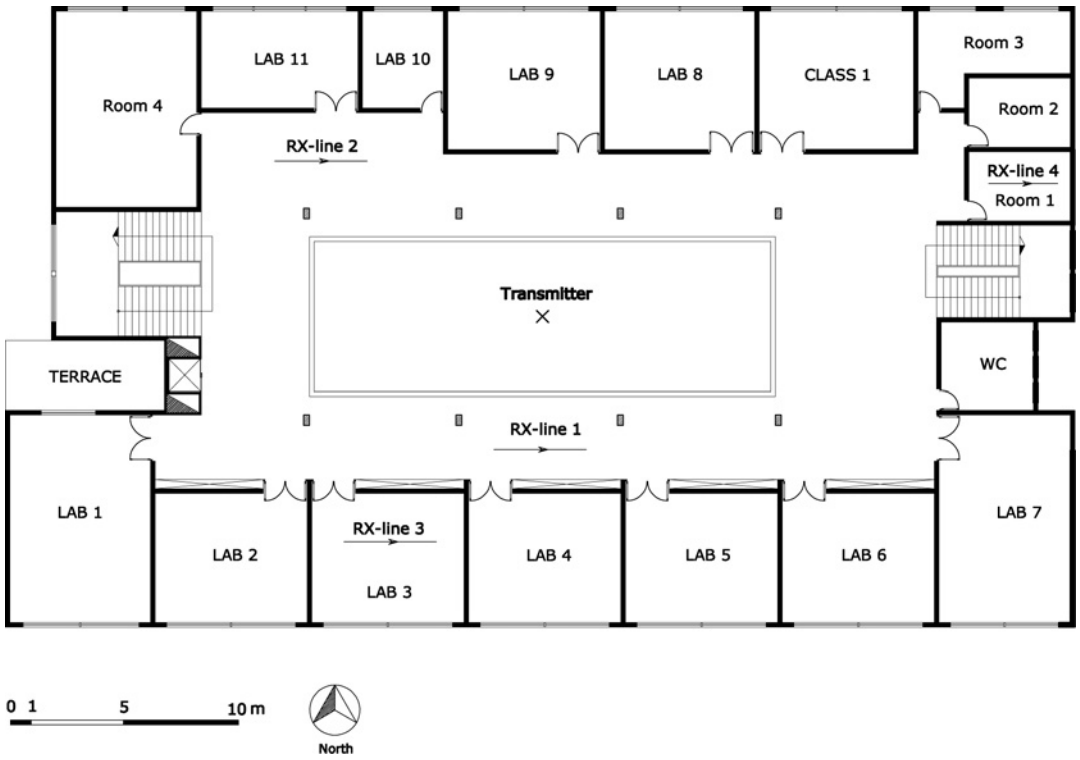

Fig. 7 *Plan of the second floor of the electrical engineering department of Sharif University of Technology*

super-sampling [9, 14] is automatically considered. This results in an extremely low number of emitted rays and potentially reduces the simulation time.

6 Numerical results and discussion

In this section, the results of using the modified wavefront decomposition method are presented and the efficiency in the simulation time is evaluated. Fig. 7 shows the plan of the second floor of the Electrical Engineering Department of Sharif University of Technology. Several laboratories and rooms are located in this floor. There are concrete ceiling and floor, brick walls, wooden doors, glass windows and metallic boxes in the environment whose electrical properties and thicknesses are summarised in Table 1. The permitivitties of the building materials are taken from [19]. The height of the ceiling from the floor is 2.8 m in the main hall and 3.5 m in the labs and rooms. The transmitting antenna is mounted on the ceiling in the centre of the main hall. It is a vertically polarised half-wavelength dipole antenna which operates at 2.45 GHz and radiates an radio frequency (RF) power of 40 mW.

A fully 3D high-resolution ray-tracing code using the SBR method has been previously prepared by the authors. The accuracy and proper functionality of this ray-tracing code have been validated in [16] and, therefore its results can be reliably used as a reference solution. For generating the source rays in this reference solution, the traditional method of using a tessellated icosahedron is used [2, 3]. The tessellation frequency of the source is selected $N = 150$ which is equivalent to $10N^2 + 2 = 225\,002$ source rays and $20N^2 = 450\,000$ energy tubes. Selecting such a high tessellation frequency is necessary to ensure the accuracy of the results in this relatively large and complex environment. In contrast, the modified wavefront decomposition method models the source with the low tessellation frequency of $N = 10$ which is equivalent to only 1002 launched rays and 2000 energy tubes. The receiver locations are considered along two LOS paths in the main hall (RX-line 1 and RX-line 2) and two non-line-of-site (NLOS) paths in a lab (RX-line 3) and a room (RX-line 4). The channel parameters are calculated for 150 equidistant points along each path. The height of the receiver is considered 1 m from the floor at which the wireless LAN users are typically located. For indoor scenarios that wave penetration inside the walls is noticeable, the maximum number of bounces in the ray-tracing simulation is usually selected in the range of 4–7 [5, 6]. This is based on proper convergence of the simulation results. Careful investigation of the results of the reference solution ensured the convergence after six bounces. Thus, the maximum number of bounces is selected six for this simulation. All simulations are performed using a PC with 2 GHz Intel Core 2 Duo CPU and 2 GB of RAM. The received power and rms delay spread of the channel are calculated at receiver locations in the reference solution and modified wavefront decomposition method and compared in Figs. 8 and 9 for LOS and NLOS cases, respectively. The simulation time is provided in Table 2. Excellent agreements between each set of the curves of Figs. 8 and 9 are observed. Besides, the simulation time is reduced by a factor of more than 6. The reason is that much less rays are traced in the modified wavefront decomposition method than the reference solution. In other words, the presented method eliminates

Table 1 Characteristics of walls used in the simulation

Environment object	ε_r	Thickness, cm
concrete ceiling and floor	$7.90 - j0.65$	60
brick walls	$5.20 - j0.14$	20
metallic boxes	$1 - j(9 \times 10^8)$	–
wooden doors	$3 - j0$	4
glass windows	$3 - j0$	0.4

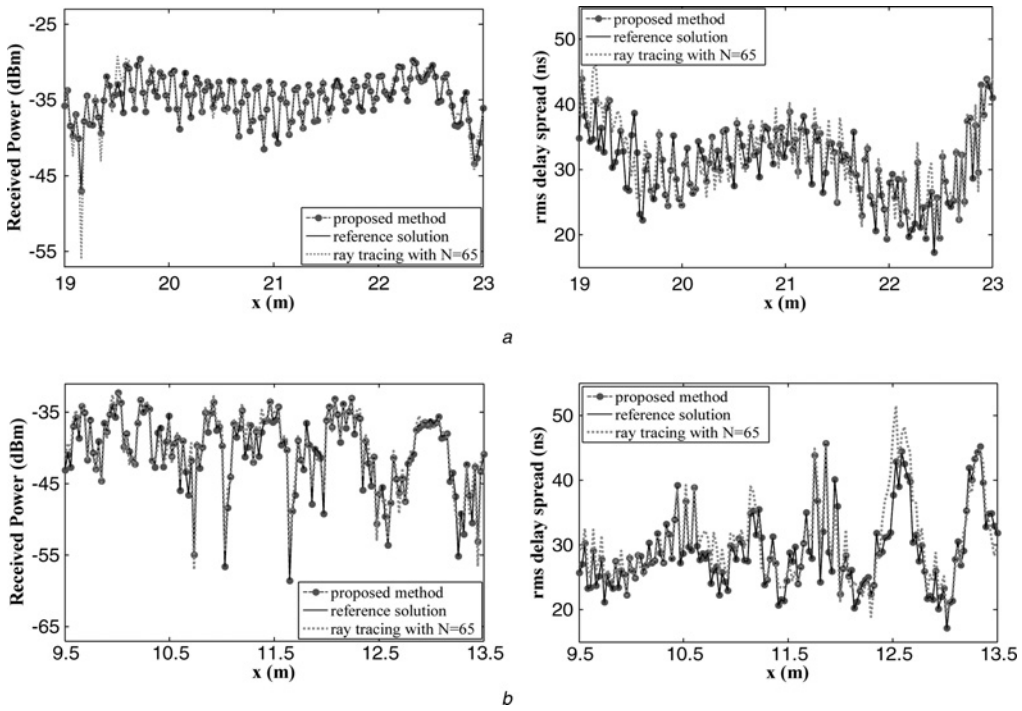

Fig. 8 *Received power and rms delay spread along LOS paths*

a RX-line 1
b RX-line 2

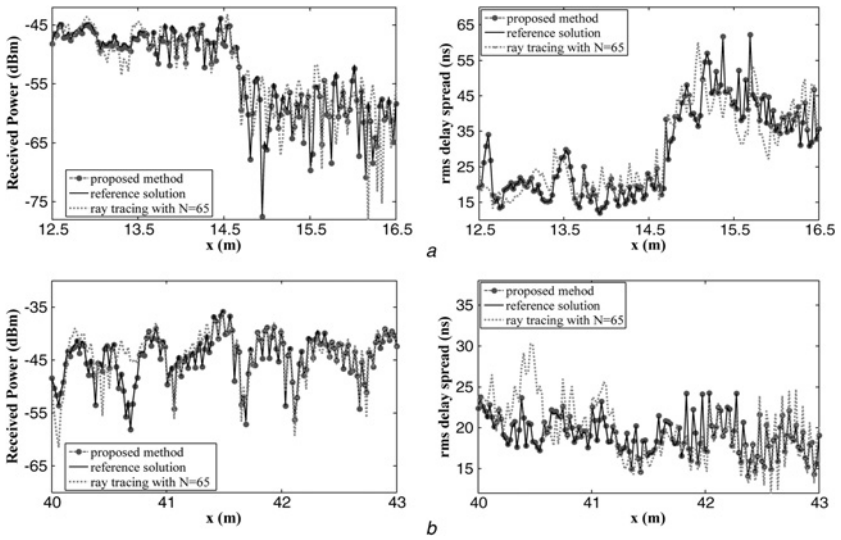

Fig. 9 *Received power and rms delay spread along NLOS paths*

a RX-line 3
b RX-line 4

the requirement of performing very high-resolution ray tracing without compromising the accuracy.

In Figs. 8 and 9, another set of graphs is depicted which shows the results of a fully 3D ray-tracing simulation with a lower tessellation frequency; that is, with $N = 65$ (42 252 launched rays). This special tessellation frequency is selected because its simulation time almost equals the simulation time of the modified wavefront decomposition method. Table 3 shows the statistical characteristics (mean and standard deviation) of the relative difference between the results of this new simulation with respect to the reference solution. The statistical characteristics of the relative difference between the results of the modified wavefront decomposition method with respect to

Table 2 Simulation time and the speedups of different acceleration techniques

Method	Simulation time	Speedup, %
reference solution	1 h 20 min	–
modified wavefront decomposition method	12 min	667
wavefront decomposition method	31 min	258
BSP	45 min	178
modified wavefront decomposition method + BSP	7 min	1142

doi: 10.1049/iet-map.2011.0264

Table 3 Mean and standard deviation (SD) of the relative difference between the results of ray tracing with $N = 65$ and modified wavefront decomposition method with respect to the reference solution

Channel parameter	Received power		RMS delay spread	
Statistical moment	Mean, %	SD, %	Mean, %	SD, %
A. Ray tracing with N = 65 results				
RX-line 1	0.92	1.65	3.59	5.49
RX-line 2	1.24	1.90	2.95	3.64
RX-line 3	3.31	4.99	14.1	17.3
RX-line 4	2.54	3.68	6.72	9.21
B. Modified wavefront decomposition method results				
RX-line 1	0.26	0.29	0.24	0.28
RX-line 2	0.25	0.29	0.26	0.30
RX-line 3	0.52	0.61	0.48	0.56
RX-line 4	0.50	0.57	0.51	0.58

the reference solution are also provided in this table. It is evident from Figs. 8 and 9 and Table 3 that the result of the modified wavefront decomposition method follows the reference solution much better than that of fully 3D ray-tracing simulation with $N = 65$, specially in the NLOS case. Therefore for the same simulation time, the modified wavefront decomposition method performs much better than a fully 3D ray-tracing simulation with a lower tessellation frequency.

The modified wavefront decomposition method provides better speedup than the previously proposed wavefront decomposition method [15, 16]. To show this, the wireless channel parameters are calculated over the aforementioned receiving locations using the wavefront decomposition method. The simulation starts with the tessellation frequency of $N = 38$ which is selected according to the location of transmitting antenna and its distance from the strong reflectors of the environment (metallic boxes) [15]. The tessellation frequency of the source is doubled at the end of each iteration and hence, by running the tracing process three times, the final tessellation frequency of $N = 152$ is achieved. This tessellation frequency is about the same as that of the reference solution. The simulation time is provided in Table 2. As we can see, the speedup obtained by using the modified wavefront decomposition method is more than the traditional wavefront decomposition method. The reason is that the modified wavefront decomposition method runs only once, whereas the wavefront decomposition method needs to iterate several times to yield the same accuracy.

We mentioned in Section 5 that the modified wavefront decomposition method can be simultaneously used with the previously published acceleration techniques such as BSP or TGRT. To show the consistency of the two types of acceleration techniques in concurrent application, the above simulation is performed in three different situations. First, our proposed method is only used. Second, the bounding-volume-based BSP method [11] is only used. Third, the two methods are applied concurrently. The results are provided in Table 2. A speedup of more than 11 times with respect to the reference solution is observed. Thus, a lot of saving in the simulation time is obtained by concurrent application of the modified wavefront decomposition method and the BSP technique.

7 Conclusions

The modified wavefront decomposition method has been presented in this paper as a new and very efficient acceleration technique for ray tracing. The method includes the effects of all multiple reflected and/or refracted energy tubes and efficiently finds the exact propagation paths towards the receiver. By using the modified wavefront decomposition method, the necessity for modelling the source with a large number of rays is eliminated without compromising the accuracy. Hence, a large saving in the simulation time can be achieved.

For validating the proposed method, a typical indoor scenario has been simulated. A very good speedup with respect to the reference solution (fully 3D high-resolution ray-tracing simulation) has been achieved. The simulation results show that the modified wavefront decomposition method results in a better simulation time reduction compared to the traditional wavefront decomposition method. Furthermore, the modified wavefront decomposition method and the binary space partitioning can be used simultaneously to yield further speedup.

The formulation of the modified wavefront decomposition method potentially allows non-uniform generation of the rays around the transmitter. This is a desirable way of source modelling since it adaptively generates less rays in directions where the geometrical complexity of the environment is low. Consequently more reduction in the simulation time is achievable. Preparing an efficient code for such source modelling scheme is the next stage of this research.

8 Acknowledgments

The authors would like to thank Iran Telecommunication Research Center for supporting this research. Special thanks are also given to Mr. Salman Parsa for helping the authors in developing the computer codes of the modified wavefront decomposition method. His brilliant comments also led to the development of a set of formulas presented in this paper. The authors also thank the anonymous reviewers for their constructive comments and suggestions.

9 References

1 McKown, J., Hamilton, J.R.L.: 'Ray tracing as a design tool for radio networks', *IEEE Netw. Mag.*, 1991, **5**, (6), pp. 27–30
2 Seidel, S.Y., Rappaport, T.S.: 'Site-specific propagation prediction for wireless in-building personal communication system design', *IEEE Trans. Veh. Technol.*, 1994, **43**, (4), pp. 879–891
3 Chen, S.-H., Jeng, S.-K.: 'An SBR/image approach for radio wave propagation in indoor environments with metallic furniture', *IEEE Trans. Antennas Propag.*, 1997, **45**, (1), pp. 98–106

4 Tiberi, G., Bertini, S., Malik, W., Monorchio, A., Edwards, D., Manara, G.: 'Analysis of realistic ultrawideband indoor communication channels by using an efficient ray-tracing based method', *IEEE Trans. Antennas Propag.*, 2009, **57**, (3), pp. 777–785

5 Tiberi, G., Bertini, S., Monorchio, A., Giannetti, F., Manara, G.: 'Computationally efficient ray-tracing technique for modelling ultrawideband indoor propagation channels', *IET Microw. Antennas Propag.*, 2009, **3**, (3), pp. 395–401

6 Agelet, F.A., Formella, A., Hernando Rabanos, J.M., Isasi de Vicente, F., Fontan, F.P.: 'Efficient ray-tracing acceleration techniques for radio propagation modeling', *IEEE Trans. Veh. Technol.*, 2000, **49**, (6), pp. 2089–2104

7 Catedra, M.F., Perez, J., Saez de Adana, F., Gutierrez, O.: 'Efficient ray-tracing techniques for three-dimensional analyses of propagation in mobile communications: application to picocell and microcell scenarios', *IEEE Antennas Propag. Mag.*, 1998, **40**, (2), pp. 15–28

8 Tan, S., Tan, H.: 'A microcellular communications propagation model based on the uniform theory of diffraction and multiple image theory', *IEEE Trans. Antennas Propag.*, 1996, **44**, (10), pp. 1317–1326

9 Suzuki, H., Mohan, A.S.: 'Ray tube tracing method for predicting indoor channel characteristics map', *Electron. Lett.*, 1997, **33**, (17), pp. 1495–1496

10 Glassner, A.S.: 'An overview of ray tracing' (Academic Press Ltd., London, UK, 1989)

11 Torres, R.P., Valle, L., Domingo, M., Loredo, S.: 'An efficient ray-tracing method for radiopropagation based on the modified BSP algorithm'. IEEE VTS 50th Vehicular Technology Conf., VTC 1999 – Fall, Amsterdam, Netherlands, September 1999, vol. 4, pp. 1967–1971

12 Yun, Z., Iskander, M.F., Zhang, Z.: 'A fast indoor/outdoor ray tracing procedure using combined uniform rectangular and unstructured triangular grids'. IEEE Antennas and Propagation Society Int. Symp., Salt Lake City, UT, USA, July 2000, vol. 2, pp. 1134–1137

13 Yun, Z., Zhang, Z., Iskander, M.: 'A ray-tracing method based on the triangular grid approach and application to propagation prediction in urban environments', *IEEE Trans. Antennas Propag.*, 2002, **50**, (5), pp. 750–758

14 Rajkumar, A., Naylor, B.F., Feisullin, F., Rogers, L.: 'Predicting RF coverage in large environments using ray-beam tracing and partitioning tree represented geometry', *Wirel. Netw.*, 1996, **2**, (2), pp. 143–154

15 Mohtashami, V., Shishegar, A.A.: 'Efficient shooting and bouncing ray tracing using decomposition of wavefronts', *IET Microw. Antennas Propag.*, 2010, **4**, (10), pp. 1567–1574

16 Mohtashami, V., Shishegar, A.A.: 'Accuracy and computational efficiency improvement of ray tracing using line search theory', *IET Microw., Antennas Propag.*, 2010, **4**, (9), pp. 1290–1299

17 Balanis, C.A.: 'Advanced engineering electromagnetics' (John Wiley and Sons, New York, NY, USA, 1989)

18 Ji, Z., Li, B.-H., Wang, H.-X., Chen, H.-Y., Sarkar, T.: 'Efficient ray-tracing methods for propagation prediction for indoor wireless communications', *IEEE Antennas Propag. Mag.*, 2001, **43**, (2), pp. 41–49

19 Bernardi, P., Cicchetti, R., Testa, O.: 'An accurate UTD model for the analysis of complex indoor radio environments in microwave WLAN systems', *IEEE Trans. Antennas Propag.*, 2004, **52**, (6), pp. 1509–1520

doi: 10.1049/iet-map.2011.0264